Journal of Energy Storage 84 (2024) 110883

Contents lists available at ScienceDirect

Journal of Energy Storage

journal homepage: www.elsevier.com/locate/est

Research papers

Investigation of structural, electronic, elastic, vibrational, thermodynamic, and optical properties of Mg_2NiH_4 and Mg_2RuH_4 compounds used in hydrogen storage

Çağatay Yamçıçıer [a], Cihan Kürkçü [b,*]

[a] Department of Electricity and Energy, Osmaniye Korkut Ata University, Osmaniye, Türkiye
[b] Department of Electronics and Automation, Kırşehir Ahi Evran University, Kırşehir, Türkiye

ARTICLE INFO

Keywords:
Structural properties
Electronic properties
Elastic properties
Phonon
Thermodynamic
Optical properties

ABSTRACT

Structural, electronic, elastic, vibrational, thermodynamic, and optical properties of Mg_2XH_4 (X = Ni, Ru) compounds were investigated using density functional theory in the presence of zero temperature and pressure. Under ambient conditions, the Mg_2NiH_4 crystallizes in an orthorhombic type structure with space group Pccn and there are 56 atoms in its unit cell. Mg_2RuH_4 crystallizes in an orthorhombic type structure with space group Cmcm and contains 28 atoms in its unit cell. In addition, electronic band structure calculations were made for the orthorhombic structures of these two compounds. Mg_2NiH_4 is a direct band gap semiconductor of 1.3479 eV, while Mg_2RuH_4 is a semiconductor with an indirect band gap of 0.8768 eV. To understand whether the studied structures of Mg_2XH_4 are dynamically stable, phonon calculation was performed and both structures were found to be stable. In addition, the second-order independent elastic constant values, which give information about the hardness of Mg_2XH_4 and whether it is mechanically stable or not, were also calculated. From the elastic constant results obtained, Mg_2XH_4 was found to be mechanically stable in both structures. Some stiffness constants such as Bulk modulus (B), Shear modulus (G), Young's Modulus (E), and Poisson's ratio (υ) were also calculated from elastic constant values. According to the B/G ratio, the material was found to be brittle in both structures. It was also observed that the atoms forming the structures according to the Poisson ratio were connected by ionic bonds. In addition, thermo-physical and optical calculations of the compounds were also examined to have more information about the physical properties of Mg_2XH_4.

1. Introduction

The rising population and demand for energy to meet our everyday needs have prompted global policymakers, governments, and scientists to express alarm. The depletion of oil reserves, price volatility, and environmental harm caused by production and usage are significant challenges that demand urgent attention and investment. There is a pressing necessity to examine energy sources that are abundant, inexpensive, and environmentally sustainable. Hydrogen energy is suggested and considered essential for addressing these issues. Hydrogen can function as an energy carrier in fixed power facilities, fuel cells, and portable devices [1].

The discovery of hydrogen storage materials is one of the most important steps for the development of the clean energy system of the future. The proliferation of Pure Electric Vehicles (PEVs) and Hybrid Electric Vehicles (HEVs) is considered a viable approach to address the aforementioned concerns. Nevertheless, the widespread adoption of electric vehicles is contingent upon the performance and cost efficiency of their respective battery systems. The nickel-metal hydride (Ni/MH) secondary battery is a promising on-board battery system for long-term use, offering numerous advantages including good overcharge/over-discharge capability, impressive rate capacity, substantial energy density, extended cycle life, and environmental sustainability [2–5].

Various alloys have been used to improve the hydrogen absorption and desorption properties of the materials [6–10]. The magnesium-based alloys used in this study are considered to be one of the most suitable materials for hydrogen storage, due to their hydrogen storage capacity, lower cost compared to alternative systems, and most importantly, the abundance of magnesium in the earth's crust [11]. Among these alloys, Mg_2Ni alloy attracts more attention due to its relatively

* Corresponding author.
E-mail address: ckurkcu@ahievran.edu.tr (C. Kürkçü).

https://doi.org/10.1016/j.est.2024.110883
Received 29 December 2023; Received in revised form 4 February 2024; Accepted 7 February 2024
Available online 13 February 2024
2352-152X/

high hydrogen storage capacity and favorable thermodynamics [12,13]. In the presence of moderate temperature and pressure, Mg_2Ni absorbs hydrogen and forms a new hydride. This hydride is Mg_2NiH_4 and it contains 3.6 wt% hydrogen. As a result of the alloying of pure magnesium with Ni due to the catalytic activity of transition metals, the hydrogen absorption rate of magnesium increases significantly.

Reilly and Wiswall first discovered the reversible hydrogen adsorption ability of Mg_2Ni in 1968, forming a ternary hydride, Mg_2NiH_4 [14]. Thus, the physics and chemistry of ternary hydrides have been a subject of study since this date [6–10]. The research conducted by Garcia et al. [15] involves the use of density functional theory to study cubic Mg_2NiH_4, a compound consisting of seven atoms within its basic unit cell. Neutron diffraction was used to investigate the structural properties of Mg2NiH4 [16]. A study on the thermodynamic, electronic, and optical properties of the monoclinic structure of Mg_2NiH_4 was carried out by Myers et al. [17].

Mg_2XH_4 is of interest in the field of hydrogen storage for fuel cells and other hydrogen-based energy applications due to their ability to reversibly absorb and release hydrogen under certain conditions. Mg_2NiH_4 is a metal hydride that can absorb and release hydrogen reversibly. This property is crucial for hydrogen storage systems as it allows for the controlled storage and release of hydrogen gas. Ruthenium-based hydrides, such as Mg_2RuH_4, have been investigated for their catalytic properties, which can improve the kinetics of hydrogen absorption and desorption in magnesium hydride systems. The addition of ruthenium can act as a catalyst, enhancing the performance of magnesium hydride.

Over the past few years, numerous materials have been examined for their ability to store hydrogen. However, comprehending the various characteristics of hydrogen storage materials is crucial, given that each material exhibits distinct hydrogenation/dehydrogenation behaviors. To fully harness the potential of hydrogen energy, it is crucial to thoroughly investigate the physical properties of materials, including their crystal structures, hydrogenation capabilities, electronic characteristics, elastic properties, anisotropic properties, and thermodynamic properties [18–20].

For instance, by modeling the material's behavior under pressure, we can gain insight into how it would react when subjected to hydrogen storage pressure. The utilization of reversible hydrogen storage materials has the potential to bring about a significant transformation in the storage of hydrogen and the adoption of hydrogen energy in daily life. Additionally, it can contribute to reducing the average global temperature, thereby mitigating the impacts of global warming. Therefore, there is still a need to discover new kinds of materials. The properties of Mg_2XH_4 (X = Ni, Ru) compounds have been investigated using density functional theory calculations. This study is the first to examine their structural, elastic, isotropic, electronic, dynamic, thermodynamic, and optic properties. Gravimetric hydrogen densities, hydrogen desorption temperatures, and enthalpies of formation have also been estimated. The current literature lacks any experimental or theoretical exploration of these material features. Hence, this study will significantly enhance the current body of literature and understanding of solid-state hydrogen storage.

This work is organized as follows. In Section 2 we present the ab initio calculating method. The results obtained for the calculated structural properties of the orthorhombic hydride Mg_2XH_4, electronic band structure, density of states, dynamic and mechanic properties, elastic anisotropy properties, Thermo-physical properties, and optic properties are described in Section 3. The conclusions are stated in Section 4.

2. Methods

The Siesta Package Program was used to analyze various physical aspects of the Mg_2XH_4 compound, including its structural, electronic, elastic, dynamic, optical, and thermo-physical characteristics. This analysis was conducted within the framework of Density Functional Theory [21]. The exchange-correlation energy [22] was selected to be calculated using the Perdew-Burke-Ernzerhof (PBE) parameter in the Generalized Gradient Approximation (GGA). Before starting the calculations, necessary geometry optimizations were performed. The most stable structures with minimum energy were obtained for the simulation study. And all calculations were performed on these structures. The computations utilized Troullier Martins type norm-conserving pseudopotentials for the Mg, Ni, Ru, and H atoms [23]. Furthermore, the calculations were conducted using the double zeta polarized basis set. After the optimization process, the mesh cut-off energy value was determined to be 300 Raydberg. The Monkhorst-Pack method was used to discretize the Brillouin zones (BZ) for Mg_2NiH_4 and Mg_2RuH_4, employing a k-point mesh [24]. The k-point mesh sizes were 8x6x4 for Mg2NiH4 and 6x4x8 for Mg_2RuH_4. The conjugate-gradient (CG) method was employed to carry out structural optimizations until the residual force applied to all atoms reached a value below 0.01 eV/Å. To analyze every step of the reduction process, we employed the KPLOT software and the RGS algorithm [25,26]. The KPLOT program, developed using the RGS algorithm, allows us to acquire comprehensive data on the space group, lattice parameter values, and atomic positions of the compounds under investigation. The stress-strain technique with the Siesta program was used to compute the second-order independent elastic constant values of Mg_2XH_4. The hardness characteristics, including the Bulk modulus, Shear modulus, Young modulus, and Poisson's ratio, were calculated using the elastic constant values to obtain precise information on the material's hardness. The DFT method has proven to be one of the most accurate methods for the computation of the electronic structure of solids [27–33].

3. Results and discussions

3.1. Structural and hydrogen storage properties

The crystal structures of Mg_2NiH_4 and Mg_2RuH_4 are orthorhombic with space group Pccn (No. 56) and Cmcm (No. 63), respectively. Fig. 1 illustrates the schematic representation of the crystal structure of Mg_2XH_4 (X = Ni, Ru). For Mg_2NiH_4, Mg, Ni, H atoms occupy the following Wyckoff positions in the unit cell: Mg1 at (¼, ¼, 0.9406), Mg2 at (¼, ¾, 0.9768), Mg3 at (0.0136, 0.2628, 0.9297), Ni at (0.8697, 0.5188, 0.8059), H1 at (0.2567, 0.5360, 0.7450), H2 at (0.6262, 0.7370, 0.8185), H3 at (0.4577, 0.5558, 0.8414), and H4 (0.1102, 0.5707, 0.9734). The unit cell contains sixteen Mg atoms, eight Ni atoms, and thirty-two H atoms. For Mg_2RuH_4, Mg, Ru, H atoms occupy the following Wyckoff positions in the unit cell: Mg1 at (0.7095, 0.1419, ¼), Ru at (0, 0.3680, ¼), H1 at (0.7413, 0.887, ¼), and H2 at (0, 0.7791, 0.5157). The unit cell contains eight Mg atoms, four Ru atoms, and sixteen H atoms. To investigate the characteristics of Mg_2XH_4 in its ground state, the geometry optimization process has been carried out at absolute zero temperature and pressure. Table 1 displays the theoretical/experimental values for the structural properties along with the results of first-principles calculations. The calculated values of lattice constants agree very well with the results of a previous study [34].

In this study, formation energy, which is a thermodynamic quantity, was calculated. Additionally, desorption temperature was calculated using another thermodynamic quantity such as formation energy and entropy. Formation energy provides information about the stability of the compound. Lower formation energy values indicate higher thermodynamic stability. The formation energy of Mg_2NiH_4 and Mg_2RuH_4 compounds are obtained using the Eq. (1).

$$\Delta H_f = E_t(Mg_2XH_4) - 2E(Mg) - E(X) - 2(H_2) \quad (1)$$

The symbol $E_t(Mg_2XH_4)$ represents the overall energy of Mg_2XH_4 hydrides. E(Mg), E(X), and $E(H_2)$ denote the ground state energies of the Mg, X (X = Ni and Ru) atom, and hydrogen molecule, respectively. Formation energies for Mg_2NiH_4 and Mg_2RuH_4 were obtained as

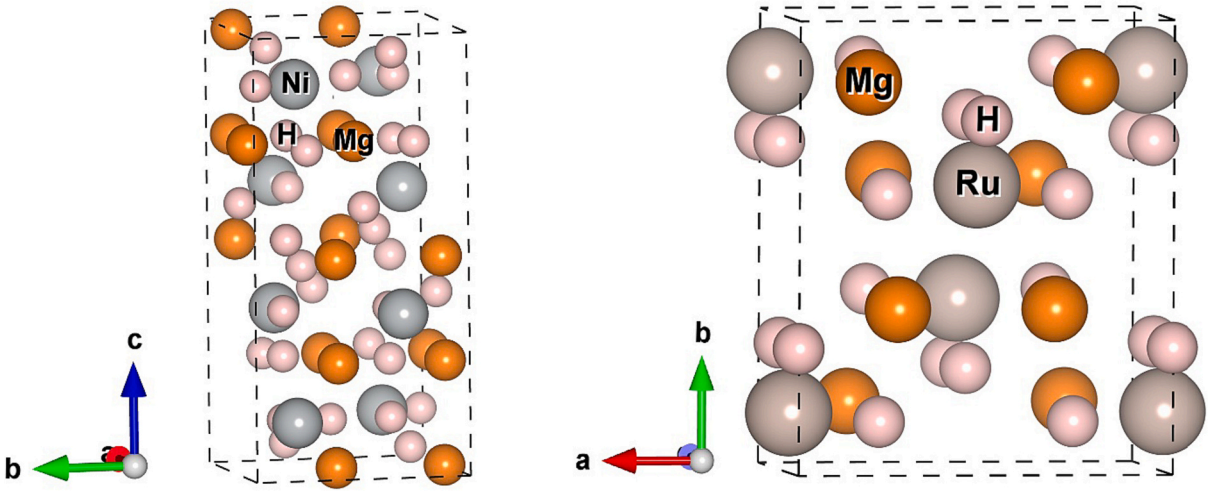

Fig. 1. Crystal structures of Mg_2NiH_4 (left) and Mg_2RuH_4 (right) compounds.

Table 1
Optimized lattice parameters (an in Å, b in Å, c in Å, and equilibrium volume V in $Å^3$) of Mg_2XH_4 (X = Ni, Ru) as compared to available theoretical data.

Material	A	b	c	V	References
Mg_2NiH_4	6.3514	6.4697	13.1600	540.77	This study
	6.3682	6.4559	13.1024	538.63	[34]
Mg_2RuH_4	7.0100	8.4162	4.8120	283.88	This study
	6.9990	8.4498	4.8159	284.82	[34]

−0.2918 and −0.4243 eV/atom, respectively. The negative formation energies indicate that the compounds Mg_2XH_4 (X = Ni and Ru) are capable of being synthesized and are thermodynamically stable. The formation energies of Mg_2XH_4 indicate that Mg_2RuH_4 is more stable than Mg_2NiH_4.

Hydrogen desorption temperature (T_{des}) is a very important parameter used to determine the temperature required to release the stored hydrogen. This value is approximately determined by the following equation [35].

$$T_{des} = \frac{\Delta H}{\Delta S} \quad (2)$$

In Eq. (2), ΔH represents the formation energy and ΔS represents the entropy change of hydrogen represented by 130.7 J mol^{-1} K^{-1} [36]. Therefore, the hydrogen desorption temperatures of Mg_2NiH_4 and Mg_2RuH_4 are 215.43, and 313.25 K, respectively. In particular, the hydrogen desorption temperatures of the Mg_2RuH_4 compound are higher than the desorption temperatures of recently published MgX_3H_8 (X = Sc, Ti, Zr), $XPtH_3$ (X = Li, Na, K, Rb) and $AeSiH_3$ (Ae = Li, K, Na, Mg) compounds [37–39].

3.2. Electronic properties

The electronic band structure is a crucial aspect of solid-state physics, as it provides insights into several material properties, including magnetic properties, electronic thermal conductivity, optoelectronic characteristics, electronic heat capacity, Hall effect, and electrical conductivity. In this study, the electronic band structure and density of the state curve of the Mg_2XH_4 were investigated along the high symmetry axes, and band gap values were calculated. In this way, the conductivity properties of the Mg_2XH_4 such as metallic, semiconductor, or insulator were calculated. From the density of state calculations, the contributions from orbitals above and below the Fermi energy level were analyzed in detail.

Fig. 2a and b illustrates the computed electronic band structure of Mg_2NiH_4 and Mg_2RuH_4 inside the first Brillouin zone under conditions of zero temperature and pressure. The band structure is shown as a function of energy ($E-E_F$) along several high symmetry directions, namely Γ- X- S- Y- Γ- Z- U- R- T- Z|X- U|Y- T|S- R, respectively. The Mg_2NiH_4 compound has a band structure that shows a direct and narrow bandgap between the highest energy level in the valence band and the lowest energy level in the conduction band at the Γ point within the material. The band structure analysis of Mg_2RuH_4 reveals the presence of an indirect bandgap, wherein the maximum of the valence band at the Γ point is separated from the minimum of the conduction band at the Z point. The determined band gap values for Mg_2NiH_4 and Mg_2RuH_4 were 1.3479 eV and 0.8768 eV, respectively. Given that both materials possess a discernible band gap, it may be inferred that they exhibit characteristics of semiconductors.

The concept of the electronic energy density of states (DOS) is employed to ascertain the quantity of potential electronic states that may be filled by an electron at each energy level within a certain energy range. The relationship between the structure of the density of states in the conduction and valence bands is intricately linked to the majority of the electrical and optical properties exhibited by crystalline solids. Furthermore, the determination of the DOS of a material is of utmost importance in understanding the individual atomic contributions to bonding and antibonding states. Fig. 3 illustrates the calculated total and partial density of states of Mg_2XH_4 in its ground state. The Fermi energy (EF) is denoted by a vertical dashed line. The semiconductor nature of the materials is evident in Fig. 3, where the absence of values intersecting the Fermi level is observed. In addition, the PDOS (Partial Density of States) of Mg, H, and X atoms was computed to get insight into their respective contributions to the overall density of states and chemical bonding. The dominant contribution in the valence band of Mg_2NiH_4 arises from the hydrogen s-orbitals within the energy range of −8 to −5. Additionally, the most significant contribution is attributed to the nickel d-orbitals within the energy range of −3 to 0. The dominant contribution in the conduction band above the Fermi level is attributed to the Ni-d orbitals. In the case of Mg_2RuH_{decom}, the valence band is primarily influenced by the presence of hydrogen states within the energy range of −9 to −6, with the most significant contribution. Additionally, the valence band is also influenced by ruthenium d-orbitals within the energy range of −3 to 0, which make a substantial contribution. The dominant contribution in the conduction band above the Fermi level is attributed to the Ru-d orbitals.

3.3. Dynamic properties

Vibrational properties provide insights into the structural

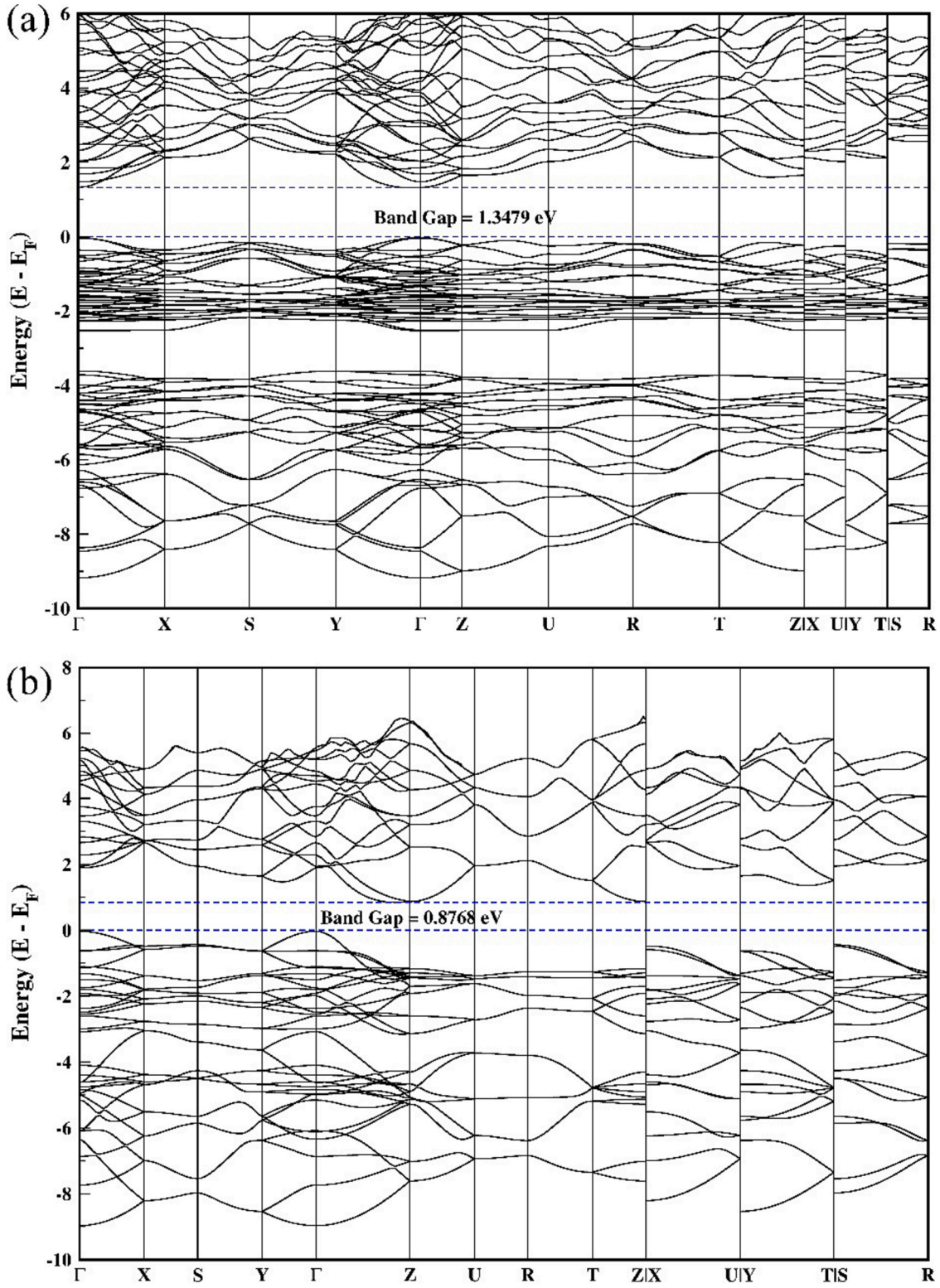

Fig. 2. Electronic band structure graph of Mg_2NiH_4 (a) and Mg_2RuH_4 (b) compounds.

characteristics of materials. Different vibrational modes are associated with specific atomic arrangements, and the analysis of these modes helps to characterize the crystal structure. Besides, the study of vibrational modes also contributes to understanding the phonon dispersion in materials. Phonons are quantized vibrational energy states, and their dispersion relation is crucial for understanding heat conduction, thermal expansion, and other thermal properties.

In the context of hydrogen storage materials, vibrational properties are crucial for understanding the interactions between hydrogen atoms and the host material. This information is essential for optimizing hydrogen storage capacities and diffusion rates. Vibrational properties are indicative of a material's thermal stability. Knowledge of these properties is crucial for designing materials that can withstand the thermal cycling associated with hydrogen absorption and desorption

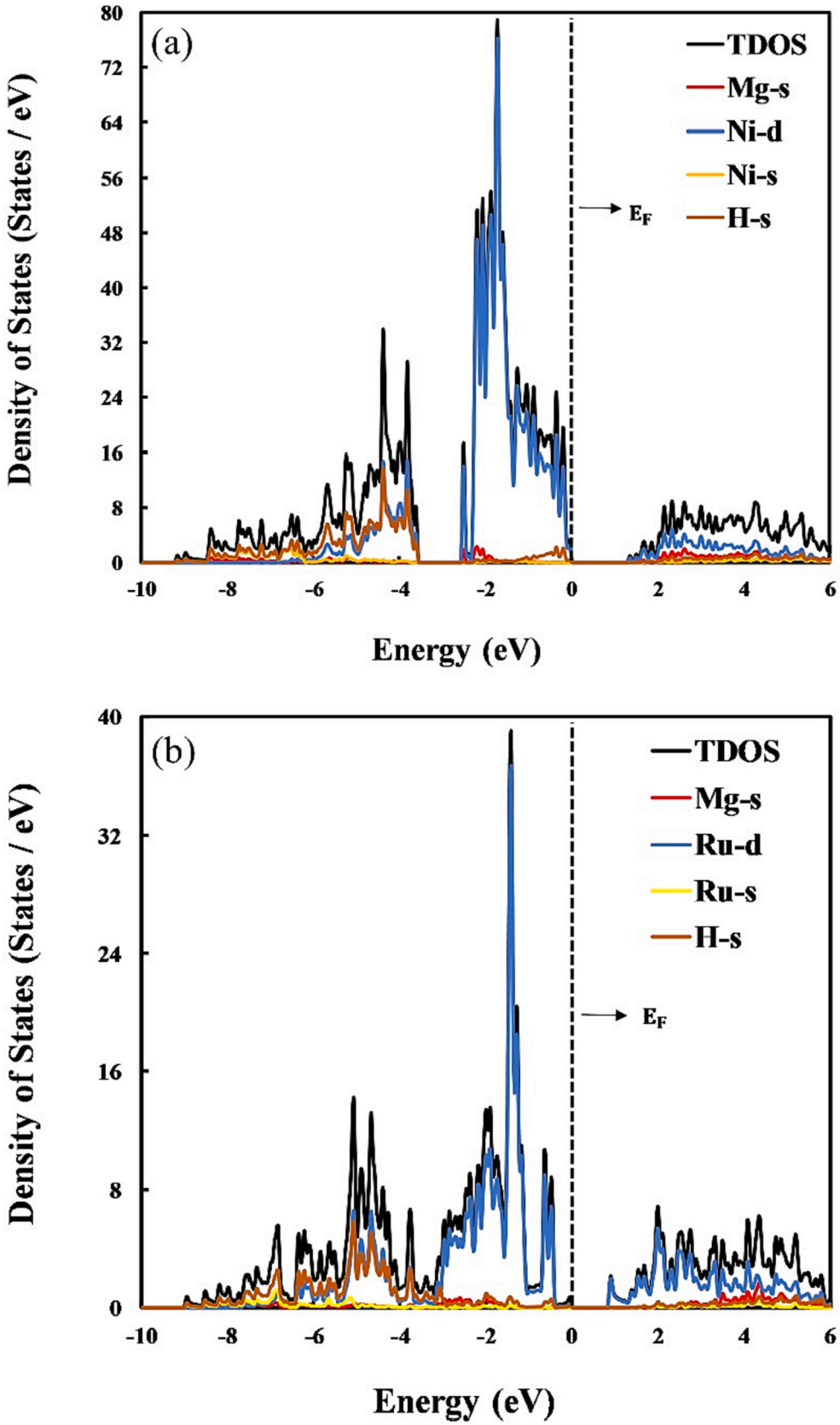

Fig. 3. Density of states graph of Mg_2NiH_4 (a) and Mg_2RuH_4 (b) compounds.

processes.

In the investigation of crystalline materials, the properties of phonons are of the utmost significance. The phonon dispersion spectra of a material can be used to either directly or indirectly determine a variety of the material's physical attributes [40]. Phonon dispersion spectra can be used to explain the structural equilibrium, transition of phase, and vibrational contribution to the thermal energy and charge transport properties of a material. The ground-state phonon dispersion curves of Mg_2XH_4 have been computed using the finite displacement approach based on density functional perturbation theory [41,42]. Fig. 4 shows the phonon dispersion spectra of Mg_2XH_4 in the Brillouin zone at zero pressure along the high symmetry axes. The compounds Mg2NiH4 and

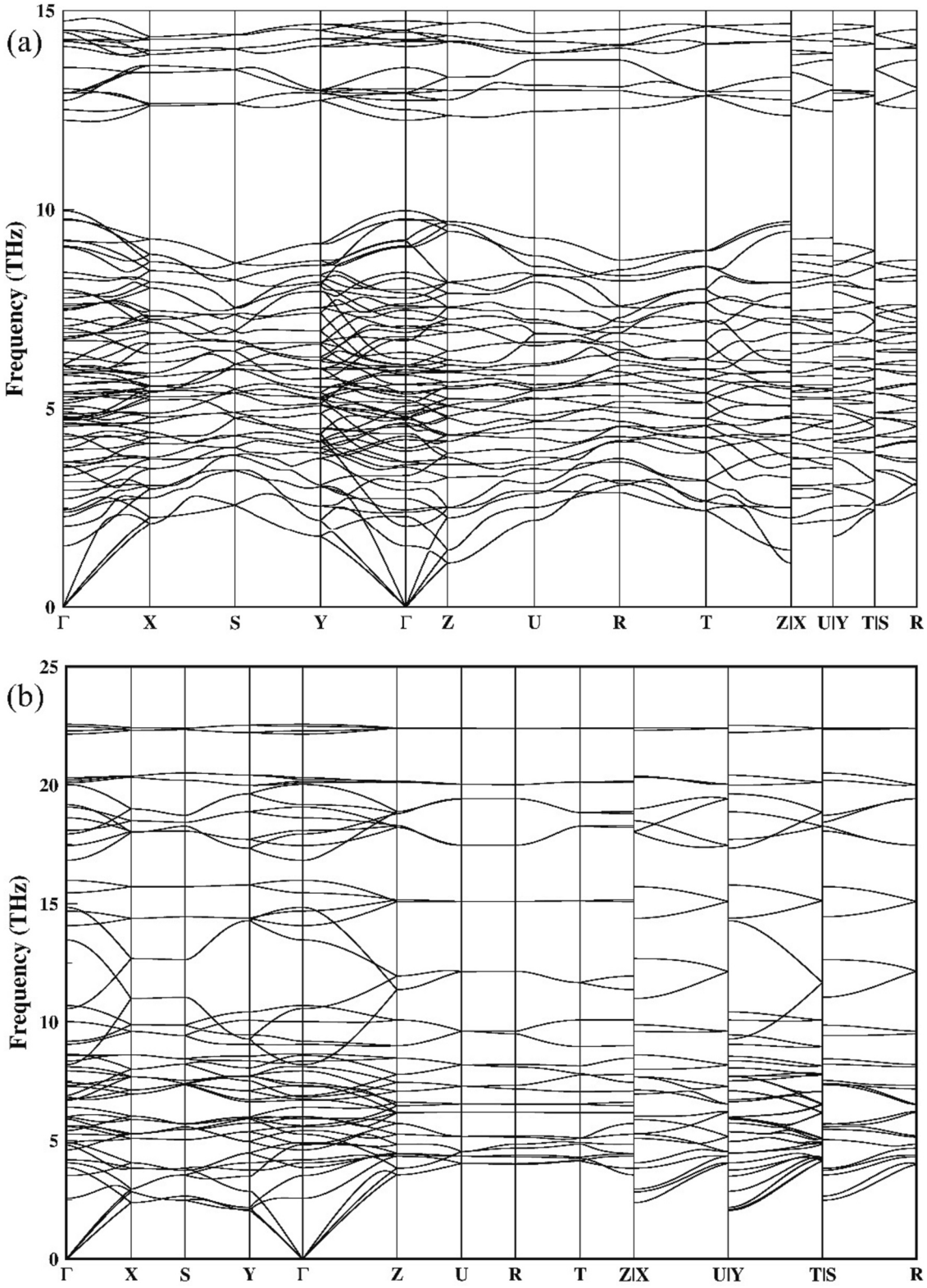

Fig. 4. Phonon graph of Mg_2NiH_4 (a) and Mg_2RuH_4 (b) compounds.

Mg2RuH4 exhibit a total of 56 atoms within each unit cell. The total number of phonon branches in the material is determined by multiplying the number of atoms in the unit cell by the number of degrees of freedom possessed by each atom. The total number of phonon branches is 168, as each atom is capable of oscillating in three axes (x, y, z). Among these branches, the number of Acoustic Phonon branches is equal to the number of degrees of freedom, which is 3. 165 branches are specifically related to Optical Phonons. Optical phonons possess greater energy compared to acoustic phonons. In phonon dispersion spectra, the presence of a negative frequency at the gamma point is usually indicative of the dynamic instability of the material. The phonon distribution spectra of both Mg_2NiH_4 and Mg_2RuH_4 are dynamically stable in both compounds as they show positive phonon frequencies throughout the Brillouin region.

3.4. Mechanic properties

Calculating the elastic properties of hydrogen storage materials is crucial for several reasons, particularly in the context of developing efficient and practical hydrogen storage systems. Hydrogen storage is a key component of hydrogen-based energy systems, which are being explored as a clean and sustainable alternative to traditional energy sources. The elastic properties play a significant role in the design, performance, and safety of these materials. Elastic properties, such as Young's modulus and bulk modulus, provide information about the material's ability to withstand deformation under external forces. Understanding these properties is essential for ensuring the structural integrity and stability of the hydrogen storage materials during cycling (absorption and desorption of hydrogen). Furthermore, knowledge of elastic properties helps also in assessing the durability and reliability of hydrogen storage materials over repeated cycles of hydrogen uptake and release. This is important for practical applications where materials undergo stress and strain during the loading and unloading of hydrogen. In addition, by understanding the elastic properties, researchers can tailor the design of hydrogen storage materials to optimize their performance. This includes choosing materials with appropriate mechanical properties to enhance the overall efficiency and longevity of the hydrogen storage system.

In summary, calculating the elastic properties of hydrogen storage materials is crucial for optimizing the design, performance, and safety of hydrogen storage systems, which, in turn, contributes to the development of reliable and efficient hydrogen-based energy solutions. The second-order independent elastic constant values obtained for the materials used in this study and the hardness constant data calculated using these values are ideal for the design of hydrogen storage systems. The elastic constant values obtained also met the Born stability criteria, which are well-known in the literature. Therefore, both materials are mechanically stable. This result is very important for the design of new hydrogen storage systems.

The elastic constants serve to create a connection between the dynamic and mechanical characteristics exhibited by crystals when subjected to stress. [43]. The provided data offers crucial insights into the crystal's reaction to external forces, as characterized by the B, bulk modulus, Y, Young's modulus, G, shear modulus, and v, Poisson's ratio. These constants play a crucial role in assessing the mechanical properties of materials and evaluating their suitability for diverse engineering applications [44,45]. Furthermore, the calculation of elastic constants has significant importance in assessing the structural and mechanical stability of materials. Table 2 displays the derived elastic constants for Mg_2XH_4. The current Born-Huang stability requirements for an orthorhombic crystal structure are presented below [46]:

$$C_{11} > 0, C_{44} > 0, C_{55} > 0, C_{66} > 0, C_{11}C_{22} > C_{12}^2, C_{11}C_{22}C_{33} + 2C_{12}C_{13}C_{23} - C_{11}C_{23}^2 - C_{22}C_{13}^2 - C_{33}C_{12}^2 > 0 \quad (3)$$

According to the data provided in Table 2, it is evident that the elastic constants exhibit non-negative values, hence fulfilling the mechanical stability criterion. This observation suggests that Mg_2XH_4 has mechanical stability. The elastic constants C_{11}, C_{22}, and C_{33} of orthorhombic crystals are recognized as key factors in determining the response to uniaxial strain and the resistance to mechanical stress along the a, b, and c axes. The results shown in Table 2 indicate that the ordering of the elastic constants for Mg_2NiH_4 is $C_{11} > C_{22} > C_{33}$, whereas for Mg_2RuH_4, the ordering is $C_{33} > C_{22} > C_{11}$. In the context of uniaxial stresses, it can be observed that Mg_2NiH_4 exhibits the most compressibility, while Mg_2RuH_4 demonstrates the lowest compressibility when subjected to stress along the c-direction. Conversely, Mg_2NiH_4 displays the lowest compressibility, while Mg_2RuH_4 exhibits the highest compressibility when subjected to stress along the a-direction.

The elastic constant C_{44} is a measure of the ability of a material to withstand shear deformation resulting from the application of tangential stress along the [001] direction in the (001) plane. If the elastic constants adhere to the subsequent condition: $C_{44} < (C_{11}, C_{22}, C_{33})$, This demonstrated that, in comparison to unidirectional compression, shear from three crystallographic axes is more effective at deforming compounds along the same directions. As seen by the data presented in Table 2, it is apparent that the sensitivity to shear deformation is higher for the examined compounds, particularly Mg_2XH_4, due to the fulfillment of this criterion. The additional elastic constants, C_{13} and C_{12}, are referred to as non-diagonal shear components and are indicative of the compound's ability to withstand deformations.

Poisson's ratio and anisotropy indicators can be obtained using different elastic modulus of elastic constants C_{ij}. The linear combination of various elastic constants can be used to get the isotropic bulk and shear modulus using Voigt's technique [47]. As per the Voight approach, the Bulk and Shear modules are denoted as B_V and G_V, correspondingly. In contrast, Reuss [48] obtains an alternative estimation for the bulk and shear modulus based on the elastic constants of a single crystal. As per the Ruess methodology, the Bulk and Shear modules are denoted as B_R and G_R, correspondingly. Subsequently, Hill [49] provided a definition stating that the Reuss approximation represents the minimum bounds of the elastic modulus in polycrystalline materials, while the Voight approximation represents the maximum bounds of the elastic modulus in polycrystalline materials. Eqs. (4) and (5) depict the expressions for the bulk modulus and shear modulus, as per Hill's definitions.

$$B = \frac{B_V + B_R}{2} \quad (4)$$

$$G = \frac{G_V + G_R}{2} \quad (5)$$

Table 3 presents the values of the B, bulk modulus, G, shear modulus, B/G, Pugh's ratio, E, Young's modulus, and v, Poisson's ratio for polycrystalline materials. The ability of a material to resist changes in length when exposed to either tension or compression is quantified by Young's modulus. Dividing the tensile stress by the tensile strain is another way to get this figure. Another interesting fact is that the covalent nature of compounds is directly proportional to their Young's modulus. The value can be determined by dividing the tensile stress by the tensile strain.

Table 2
Elastic constants, C_{ij}, of Mg_2XH_4 (X = Ni, Ru) (all in GPa).

Phases	C_{11}	C_{12}	C_{13}	C_{22}	C_{23}	C_{33}	C_{44}	C_{55}	C_{66}
Mg_2NiH_4	119.161	31.945	35.725	112.261	14.939	108.759	27.514	42.515	36.266
Mg_2RuH_4	92.194	57.428	30.366	121.013	38.400	138.822	51.116	44.681	51.855

Table 3
Elastic moduli (all in GPa), Pugh's ratio, and Poisson's ratio of Mg_2XH_4 (X = Ni, Ru).

Phases	B_V	B_R	B	G_V	G_R	G	E	B/G	υ
Mg_2NiH_4	56.16	55.417	55.787	38.43	37.023	37.726	92.360	1.478	0.224
Mg_2RuH_4	67.16	65.525	66.337	44.59	40.717	42.651	105.37	1.636	0.235

Furthermore, it can be observed that an increase in Young's modulus leads to a corresponding increase in the covalent character of the compounds [50]. Looking at Table 3, it can be said that Mg_2RuH_4 has a more covalent structure. The Pugh's ratio, which is the ratio of bulk modulus (B) to shear modulus (G), is a useful indicator for determining the ductility or brittleness of a material. Based on Pugh's ratio, a material can be classified as either ductile or brittle. If the Pugh's ratio of a material exceeds 1.75, it is considered ductile, while a Pugh's ratio below 1.75 indicates brittleness. As can be seen from Table 3, both Mg_2NiH_4 (1.478) and Mg_2RuH_4 (1.636) exhibit brittle properties. Another value known as Poisson's ratio can be used to illustrate the threshold between ductility and brittleness in a material. The threshold value, as determined by Poisson's ratio, is 0.26. The material's ductility can be determined by comparing its Poisson's ratio to a threshold value of 0.26. If the Poisson's ratio is >0.26, the material is considered ductile. Conversely, if the Poisson's ratio is less than or equal to 0.26, the material is classified as brittle. The relationship between Poisson's ratio and the type of interatomic forces in solids has been studied [51]. The dominance of bondings in a solid is associated with the range of Poisson's ratio between 0.25 and 0.50. If the ratio falls outside of the specified range, the solid is primarily influenced by non-central force interactions. Furthermore, Poisson's ratio can be used to determine whether or not a material features ionic and/or covalent bonding. Poisson's ratio for covalently and ionic bonded materials was found to have values of 0.25 and 0.10, respectively [52]. As can be seen from Table 3, it can be said that Mg_2XH_4 is brittle and the ionic bond is dominant.

The machinability index (μ^M), Kleinman parameter (ζ), and Vickers hardness (H_v), which are important mechanical performance indicators, were calculated using the following equations [53,54] and presented in Table 4.

$$\mu^M = \frac{B}{C_{44}} \tag{6}$$

$$\zeta = \frac{C_{11} + 8C_{12}}{7C_{11} + 2C_{12}} \tag{7}$$

$$H_V = 2\left(k^2 G\right)^{0.585} - 3;\ (k = G/B) \tag{8}$$

A parameter known as the machinability index (μ^M), is used to determine a material's dry lubricating nature. The lubricating property of a material is directly proportional to its lubrication quality value, μ^M. That is, the higher the μ^M, the higher the lubricating property of the material. In addition, the higher the μ^M value of a material, the higher the machinability of the material [55–59]. Considering the μ^M values presented in Table 4, it can be said that the machinability of the Mg_2NiH_4 compound is higher. The Kleinman parameter (ζ) typically falls within the range of 0 to 1. The parameter provides insight into the relative importance of bond bending and bond tension in determining the resistance to external stress. When the value of ζ approaches zero, the primary factor influencing the behavior under stress is bond stretching. Conversely, when ζ approaches 1, the dominant factor is bond bending. The Kleinman parameter for Mg_2XH_4 falls within the range of 0 to 1, indicating that both bond stretching and bond bending factors contribute to the mechanical strength of Mg_2XH_4. Hardness is an important indicator for determining the elastic and plastic properties of a material [60]. As can be seen from Table 3, it can be said that these materials are relatively hard, where the hardness values for Mg_2XH_4 are below the super hardness ($H_V \geq 40$ GPa) value. The directional bulk modulus, which refers to the bulk modulus along the a-, b-, and c-axes, and the isotropic bulk modulus (B_{relax}) [54,55] are computed using the equation provided and are displayed in Table 4.

$$B_a = a\frac{dP}{da} = \frac{\Lambda}{1 + \alpha + \beta} \tag{9}$$

$$B_b = b\frac{dP}{db} = \frac{B_a}{\alpha} \tag{10}$$

$$B_c = c\frac{dP}{dc} = \frac{B_a}{\beta} \tag{11}$$

$$B_{relax} = \frac{\Lambda}{(1 + \alpha + \beta)^2} \tag{12}$$

where

$$\Lambda = C_{11} + 2C_{12}\alpha + C_{22}\alpha^2 + 2C_{13}\beta + C_{33}\beta^2 + 2C_{23}\alpha\beta$$

and

$$\alpha = \frac{\{(C_{11} - C_{12})(C_{33} - C_{13})\} - \{(C_{23} - C_{13})(C_{11} - C_{13})}{\{(C_{33} - C_{13})(C_{22} - C_{12})\} - \{(C_{13} - C_{23})(C_{12} - C_{23})\}}$$

$$\beta = \frac{\{(C_{22} - C_{12})(C_{11} - C_{13})\} - \{(C_{11} - C_{12})(C_{23} - C_{12})\}}{\{(C_{22} - C_{12})(C_{33} - C_{13})\} - \{(C_{12} - C_{23})(C_{13} - C_{23})\}}$$

The B_{relax} value, as determined by Eq. (12), is found to be equivalent to the value obtained through the Reuss approximation. The determination of changes in the b- and c- axes relies on the parameters α and β, which are influenced by the deformation along the a-axis. The smaller value of B_c for Mg_2NiH_4, in comparison to B_a and B_b, suggests that Mg_2NiH_4 is more susceptible to compression when stress is applied in the c-direction. The smaller value of B_a compared to B_b and B_c for Mg_2RuH_4 indicates that it is more compressible in the *a*-direction. These results shown in Table 4 are recent and there are no available data to compare.

3.5. Elastic anisotropy properties

The presence of anisotropy in mechanical properties is a fundamental factor that influences the equilibrium strains and mechanical stability of a material when subjected to various types of stress. The impact of elastic anisotropy on various phenomena such as the formation of micro-scale cracks in ceramics, plastic relaxation in thin films, and the development of plastic deformation in crystals has been docu-

Table 4
Machinability index (μ^M), Kleinman parameter (ζ), Vickers hardness (H_v in GPa), bulk modulus (B_{relax} in GPa), bulk modulus along a-, b-, and c-axes (B_a, B_b, and B_c in GPa), and α and β of Mg_2XH_4 (X = Ni, Ru) compounds.

Phases	μ^M	H_v	ζ	B_{relax}	B_a	B_b	B_c	α	β
Mg_2NiH_4	2.027	6.939	0.421	55.417	219.168	149.077	147.612	1.470	1.484
Mg_2RuH_4	1.297	7.527	0.775	65.525	138.651	298.534	212.799	0.464	0.651

mented. To accurately predict the behavior of solids under different external stress conditions, it is essential to analyze the elastic anisotropy parameters [59,61]. Table 5 presents the calculated values for various factors related to anisotropy, including the A_G, percentage anisotropy in shear, A_1, A_2, and A_3, shear anisotropy factors, A, Zener anisotropy factor, A^{eq}, equivalent Zener anisotropy, A_B, percentage anisotropy in compressibility and A^U and d_E, universal anisotropy factors. The equations provided below are the commonly used equations for calculating the anisotropy factor [62,63]:

$$A = \frac{2C_{44}}{C_{11} - C_{12}} \tag{13}$$

$$A_1 = \frac{4C_{44}}{C_{11} + C_{33} - 2C_{13}} \tag{14}$$

$$A_2 = \frac{4C_{55}}{C_{22} + C_{33} - 2C_{23}} \tag{15}$$

$$A_3 = \frac{4C_{66}}{C_{11} + C_{22} - 2C_{12}} \tag{16}$$

$$A_B = \frac{B_V - B_R}{B_V + B_R} \tag{17}$$

$$A_G = \frac{G_V - G_R}{G_V + G_R} \tag{18}$$

$$A^U = \frac{B_V}{B_R} + 5\frac{G_V}{G_R} - 6 \geq 0 \tag{19}$$

$$d_E = \sqrt{A^U + 6} \tag{20}$$

$$A^{eq} = \left(1 + \frac{5}{12}A^U\right) + \sqrt{\left(1 + \frac{5}{12}A^U\right)^2 - 1} \tag{21}$$

The calculated value of A_1, A_2, and A_3 indicates the isotropic nature of the material. As presented in Table 5, the calculated A_1, A_2, and A_3 values are different from 1.0. It can be said that for these Mg_2XH_4 (X = Ni, Ru) compounds it is strongly anisotropic for shear stress along different crystal planes. If the A_B and A_G values are equal to 1, it is elastic isotropic, if the value is equal to 0, it represents the highest anisotropic. Therefore, as seen in Table 5 for Mg_2XH_4, the fact that the A_G value is greater than the A_B value for both Mg_2NiH_4 and Mg_2RuH_4 indicates that the anisotropy at shear is greater than the anisotropy at compressibility. Ranganathan and Ostoja-Starzewski [64] presented a universal anisotropic factor, indicated by A^U, that applies to all symmetries in crystals. The crystal is regarded as elastically isotropic when $A^U = 0$. Any value of A^U different than zero shows that the crystal is anisotropic. When the A^U values calculated for Mg_2XH_4 are examined, the fact that the A^U value is different from 0 indicates that it is anisotropic. For the A^{eq} value, a value of 1.0 indicates isotropic, while any value other than 1.0 indicates anisotropic. Therefore, the calculated A^{eq} values for Mg_2XH_4 indicate that the materials in the study are anisotropic. All of the anisotropy indices, as a consequence, point to the presence of structural anisotropy, which can be explained by the fact that the bond strengths vary in different directions within the crystal's unit cell.

The universal log-Euclidean index [62] can be defined by the following equation:

$$A^L = \sqrt{\left[ln\left(\frac{B_V}{B_R}\right)\right]^2 + 5\left[ln\left(\frac{C_{44}^V}{C_{44}^R}\right)\right]^2} \tag{22}$$

where

$C_{44}^R = \frac{5}{3}\frac{C_{44}(C_{11} - C_{12})}{3(C_{11} - C_{12}) + 4C_{44}}$ is the Reuss value of C_{44},

$C_{44}^V = \frac{3}{5}\frac{(C_{11} - C_{12} - 2C_{44})}{3(C_{11} - C_{12}) + 4C_{44}}$ is the Voight value of C_{44}.

Kube and Jong [65] showed that the A^L value for inorganic crystalline compounds was in the range of $0 \leq A^L \leq 10.26$ and 90 % of these compounds had a $A^L < 1$ value. It has also been suggested that the A^L value is an indication of the existence of a layered or lamellar-type configuration. A high A^L the value indicates that the material has a strong layered structure and a low A^L the value indicates a non-layered structure. Therefore, since the calculated A^L values for Mg_2XH_4 are partially low, we can say that these compounds do not have a significant layered structural configuration.

Bulk modulus anisotropies along a- and c-axes are defined as follows [54]:

$$A_{B_a} = \frac{B_a}{B_b} \tag{23}$$

$$A_{B_c} = \frac{B_c}{B_b} \tag{24}$$

Table 5 presents the calculated values of A_{B_c}, and A_{B_a}, which demonstrate that the bulk modulus for Mg_2XH_4 exhibits anisotropy along both the a- and c- axes. The results presented in Table 5 are entirely novel, with no existing estimates available for comparison.

Isotropic solids have spherical shapes for their three-dimensional (3D) direction-dependent linear compressibility, Poisson's ratio, Young modulus, and shear modulus. Any deviation from this spherical shape indicates anisotropy. In Fig. 5, we show 3D graphs generated by ELATE [66] corresponding to the directional dependence of linear compressibility, Poisson's ratio, Young modulus, and shear modulus for Mg_2XH_4 (X = Ni, Ru) compounds.

3.6. Thermo-physical properties

The Debye temperature, denoted as θ_D, corresponds to the temperature at which the crystal's maximum frequency normal mode of vibration is observed. The temperature is contingent upon the atomic mass constituent of the compound and the hardness of the crystal. θ_D is a significant thermophysical characteristic of solids that is linked to different physical factors. The parameters encompassed in this set are lattice thermal conductivity, vacancy formation energy, melting temperature, bonding strength among atoms inside the crystal, and phonon-specific heat. Acoustic modes are the only cause of vibrational excitations at low temperatures. Thus, θ_D and specific heat derived from elastic constants exhibit equivalence at low temperatures. The Debye temperature θ_D is determined by the sound velocity in the crystal, as expressed in Eq. (23) [67].

$$\theta_D = \frac{h}{k_B}\left[\left(\frac{3N}{4\pi}\right)\frac{N_A\rho}{M}\right]^{\frac{1}{3}} v_m \tag{25}$$

The given equation includes various symbols and constants. These

Table 5
Elastic anisotropy indices of Mg_2XH_4 (X = Ni, Ru) compounds.

Phases	A	A_1	A_2	A_3	A_B	A_G	A^U	d_E	A^{eq}	A^L	A_{B_a}	A_{B_c}
Mg_2NiH_4	0.630	0.703	0.889	0.865	0.006	0.018	0.203	2.490	1.504	0.323	1.470	0.990
Mg_2RuH_4	2.940	1.200	0.976	2.108	0.012	0.045	0.500	2.549	1.886	1.461	0.464	0.712

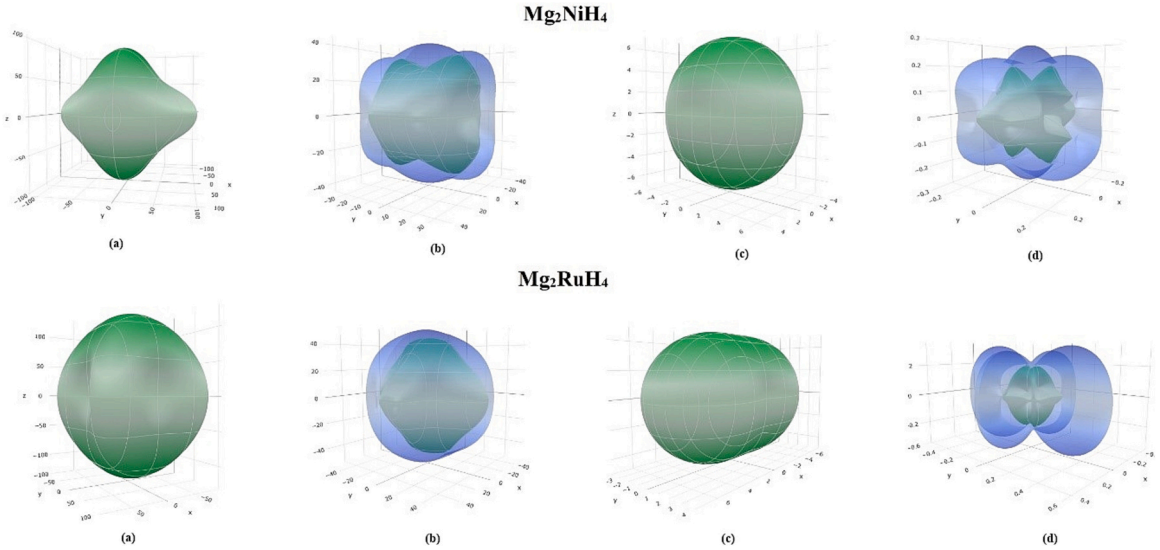

Fig. 5. Elastic modulus in 3-Dimension:Young modulus (a), shear modulus (b), linear compressibility (c), and Poisson's ratio (d) for Mg_2XH_4 (X = Ni, Ru) compounds are drawn using the graphical tool ELATE [66].

include k_B for Boltzmann's constant, h for Planck's constant, M for molar mass, N for the number of atoms within the unit cell, ρ for density, N_A for Avogadro's number, and v_m for the mean sound velocity. The value of v_m can be calculated using Eq. (26). Eq. (28) defines the variables used in the context of bulk moduli (B), shear moduli (G), longitudinal sound velocities v_l, and transverse sound velocities v_t.

$$v_m = \left[\frac{1}{3}\left(\frac{2}{v_t^3} + \frac{1}{v_l^3}\right)\right]^{-\frac{1}{3}} \tag{26}$$

where

$$v_t = \sqrt{\frac{G}{\rho}} \tag{27}$$

$$v_l = \sqrt{\frac{3B + 4G}{3\rho}} \tag{28}$$

The calculated Debye temperature θ_D, v_m, v_t and v_l values are presented in Table 6. As can be seen from Table 6, the Debye temperature of Mg_2NiH_4 is higher than that of Mg_2RuH_4. Therefore, the lattice conductivity of Mg_2NiH_4 is expected to be significantly higher than Mg_2RuH_4.

Information about the melting temperature of a substance is crucial for applications at various temperatures. A chemical with a high melting point has limited thermal expansion and high binding energy, and vice versa. Fine et al. [68] proposed the following empirical method for determining the melting temperature of solids using elastic constants:

$$T_m = 354 + 1.5(2C_{11} + C_{33}) \tag{29}$$

The calculated melting temperatures of Mg_2XH_4 are listed in Table 6. The substance with the highest melting temperature and the highest hardness also has the highest Debye temperature. This is to be anticipated, as a higher Debye temperature predicts increased melting temperature and mechanical strength as a result of stronger interatomic bonding. The melting temperature, T_m of crystalline material is proportional to its bonding energy. As can be seen from Table 5, Mg_2NiH_4 has a higher melting temperature than Mg_2RuH_4. Therefore, it can be said that the Mg_2NiH_4 compound has greater bonding energy.

Table 6
Calculated mass density (ρ in gm cm^{-3}), longitudinal, transverse, and sound velocities (vl, vt, and vm in km s^{-1}, respectively), Debye temperature (θ_D in K), and melting temperature (T_m in K) of Mg_2XH_4 (X = Ni, Ru).

Phases	ρ	v_t	v_l	v_m	θ_D	T_m
Mg_2NiH_4	2.735	3.714	6.228	4.111	574.80	874.62
Mg_2RuH_4	3.596	3.443	5.853	3.816	525.00	838.81

3.7. Optical properties

To comprehend the response of a material to electromagnetic radiation, it is essential to have a grasp on the optical parameters that are influenced by energy (or frequency). The comprehension of a material's reaction to infrared, visible, and ultraviolet spectra is essential for investigating possible optoelectronic uses. The optical characteristics that depend on energy or frequency are useful for analyzing various aspects such as energy band structure, impurity level states, excitons, localized defects, lattice vibrations, and specific magnetic excitations [69]. The purpose of this section is to calculate the frequency-dependent optical constants, including the absorption coefficient α(ω), reflectivity R(ω), and optical conductivity σ(ω), to study how Mg_2XH_4 reacts to incoming photons. The optical functions of Mg_2XH_4 were determined for photon energies up to 30 eV of the electric field, as shown in Fig. 6.

Optical conductivity refers to the property of a material that enables the movement of free charge carriers within a particular range of photon energy. The dynamic reaction of mobile charge carriers in semiconductors primarily involves electron-hole pairs that are generated by photons. Fig. 6(a) illustrates the frequency-dependent optical conductivity σ(ω) of Mg_2XH_4 as it varies with photon energy. The presence of a band gap in the materials can be inferred from Fig. 6(a), where it is observed that photoconductivity does not initiate at zero photon energy. This observation aligns with the band gap values obtained from Fig. 2 and the density of states calculations depicted in Fig. 3. The photoconductivity of both compounds exhibits a positive correlation with photon energy. It initially increases, reaching its peak value, and then gradually decreases as the energy continues to rise. Eventually, it approaches zero at approximately 30 eV. Reflection determines the amount of incoming light energy that is reflected from the material.

The reflectivity spectra for Mg_2NiH_4 and Mg_2RuH_4 begin at approximately 0.24 and 0.15, respectively, as depicted in Fig. 6(b). Based on our analysis, we have determined that the highest reflectance value for Mg_2NiH_4 is approximately 0.29, observed at an energy level of 1.80 eV. Similarly, for Mg_2RuH_4, the maximum reflectance is around 0.27, occurring at an energy level of 8.09 eV. In the visible region, the

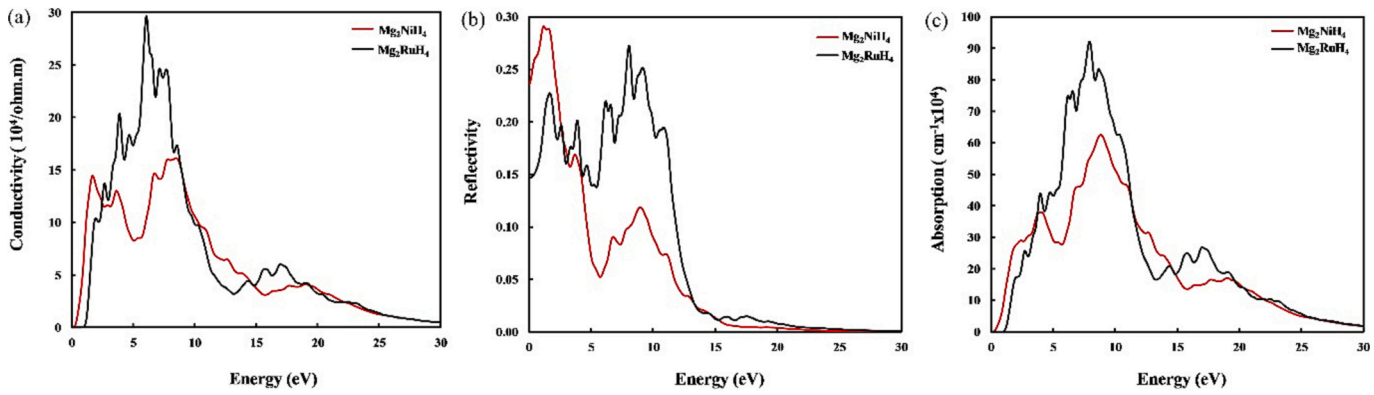

Fig. 6. The computed frequency-dependent optical conductivity (a), reflectivity spectra (b), and absorbance spectra (c) for Mg_2XH_4 (X = Ni, Ru) compounds.

reflectivity of Mg_2NiH_4 is greater than that of Mg_2RuH_4. However, in the mid-ultraviolet region, the reflectivity of Mg_2RuH_4 is higher.

Fig. 6(c) displays the absorption coefficient α(ω) for Mg_2XH_4. The absorption coefficients for Mg_2NiH_4 and Mg_2RuH_4 are approximately 1.12 eV and 0.52 eV, respectively. The evidence presented indicates that both compounds possess semiconductor properties. The onset energies exhibit a strong correlation with the bandgap values obtained from the band structure calculations. Upon examining the absorption spectra of all the materials included in the study, it is evident that the highest absorption spectrum occurs in the ultraviolet region for all polarisations of the electric field. The absorption spectra indicate that these compounds have a high affinity for absorbing UV light.

4. Conclusions

Some physical properties of the orthorhombic structures of the Mg_2XH_4 compound were calculated within the framework of density functional theory. As a result of geometry optimization, lattice parameter values in good agreement with the literature were obtained. From the electronic structure calculations, the forbidden energy band gaps for Mg_2NiH_4 and Mg_2RuH_4 were calculated as 1.3479 eV and 0.8768 eV, respectively. Thus, it was seen that both compounds have the character of semiconductor materials in the orthorhombic structure. The mechanical and dynamic properties of Mg_2XH_4 were also investigated. It was concluded that both compounds are mechanically stable since the second-order independent elastic constant values obtained satisfy the Born stability criteria. In addition, the Mg_2XH_4 compound is dynamically stable since it has no negative phonon frequency along the Brillouin zone. According to the B/G ratio and Poisson's ratio calculated from the elastic constant values, it is seen that the Mg_2XH_4 compound has brittle properties, and the atoms forming the compound are connected by ionic bonds. In addition to these studies, the thermo-physical properties of the compounds were analyzed and it was concluded that the Debye temperature of the Mg_2NiH_4 compound is higher than that of the Mg_2RuH_4 compound. Finally, some optical properties of the Mg_2XH_4 compound such as conductivity, reflectivity, and absorption coefficient were also investigated.

CRediT authorship contribution statement

Çağatay Yamçıçıer: Writing – original draft, Investigation, Funding acquisition, Conceptualization. **Cihan Kürkçü:** Writing – original draft, Methodology, Investigation.

Declaration of competing interest

The authors declare that they have no known competing financial interests or personal relationships that could have appeared to influence the work reported in this paper.

Data availability

Data will be made available on request.

Acknowledgment

This study was supported by the Osmaniye Korkut Ata University under Scientific Research Project (BAP) No: OKÜBAP-2022-PT1-002.

References

[1] S. Al, C. Kurkcu, C. Yamcicier, High pressure phase transitions and physical properties of Li2MgH4; implications for hydrogen storage, Int. J. Hydrogen Energy 45 (7) (2020) 4720–4730.
[2] L. Schlapbach, A. Züttel, Hydrogen-storage materials for mobile applications, nature 414 (6861) (2001) 353–358.
[3] S. Ovshinsky, M. Fetcenko, J. Ross, A nickel metal hydride battery for electric vehicles, Science 260 (5105) (1993) 176–181.
[4] Y. Liu, et al., Advanced hydrogen storage alloys for Ni/MH rechargeable batteries, J. Mater. Chem. 21 (13) (2011) 4743–4755.
[5] Z. Cao, et al., Enhanced discharge capacity and cycling properties in high-samarium, praseodymium/neodymium-free, and low-cobalt A2B7 electrode materials for nickel-metal hydride battery, Int. J. Hydrogen Energy 40 (1) (2015) 451–455.
[6] S. Goren, et al., NMR study of hydrogen diffusion and phase determination of the Mg2NiH x system, J. Chem. Phys. 73 (10) (1980) 4758–4764.
[7] H. Blomqvist, et al., Competing stabilisation mechanisms in Mg2NiH4, J. Alloys Compd. 330 (2002) 268–270.
[8] H. Fujii, S. Orimo, K. Ikeda, Cooperative hydriding properties in a nano- structured Mg2Ni–H system, J. Alloys Compd. 253 (1997) 80–83.
[9] S.-I. Orimo, H. Fujii, Effects of nanometer-scale structure on hydriding properties of Mg Ni alloys: a review, Intermetallics 6 (3) (1998) 185–192.
[10] P. Tessier, E. Akiba, Decomposition of nickel-doped magnesium hydride prepared by reactive mechanical alloying, J. Alloys Compd. 302 (1–2) (2000) 215–217.
[11] D. Noreus, L. Olsson, The structure and dynamics of hydrogen in Mg2NiH4 studied by elastic and inelastic neutron scattering, J. Chem. Phys. 78 (5) (1983) 2419–2427.
[12] Z. Gavra, et al., Allotropic transitions of magnesium nickel hydride (Mg2NiH4), Inorg. Chem. 18 (12) (1979) 3595–3597.
[13] P. Zolliker, et al., Structural studies of the hydrogen storage material Mg/sub2/NiH/sub 4/. 2. Monoclinic low-temperature structure, Inorg. Chem.;(United States) 25 (20) (1986).
[14] J.J. Reilly Jr., R.H. Wiswall Jr., Reaction of hydrogen with alloys of magnesium and nickel and the formation of Mg2NiH4, Inorg. Chem. 7 (11) (1968) 2254–2256.
[15] G. Garcia, J. Abriata, J. Sofo, Calculation of the electronic and structural properties of cubic Mg 2 NiH 4, Phys. Rev. B 59 (18) (1999) 11746.
[16] K. Yvon, J. Schefer, F. Stucki, Structural studies of the hydrogen storage material Mg2NiH4. 1. Cubic high-temperature structure, Inorg. Chem. 20 (9) (1981) 2776–2778.
[17] W. Myers, et al., Calculation of thermodynamic, electronic, and optical properties of monoclinic Mg 2 NiH 4, J. Appl. Phys. 91 (8) (2002) 4879–4885.
[18] C. Li, X. Zhang, F. Wang, Influence of TM elements on the mechanical and thermodynamic properties of Hf2Si intermetallics, Vacuum 220 (2024) 112793.
[19] K. Wang, X. Zhang, F. Wang, Exploring the electronic, mechanical, anisotropic and optical properties of the Sc-Al-C MAX phases from a first principles calculations, Chem. Phys. Lett. 836 (2024) 141024.
[20] C. Li, X. Zhang, F. Wang, The lattice vibration, mechanical anisotropy, stress-strain behavior and electronic properties of HfxSiy phases: a first-principles study, Vacuum 212 (2023) 112012.
[21] P. Ordejón, E. Artacho, J.M. Soler, Self-consistent order-N density-functional calculations for very large systems, Phys. Rev. B 53 (16) (1996) R10441.

[22] J.P. Perdew, K. Burke, M. Ernzerhof, Perdew, burke, and ernzerhof reply, Phys. Rev. Lett. 80 (4) (1998) 891.
[23] N. Troullier, J.L. Martins, Efficient pseudopotentials for plane-wave calculations, Phys. Rev. B 43 (3) (1991) 1993.
[24] H.J. Monkhorst, J.D. Pack, Special points for Brillouin-zone integrations, Phys. Rev. B 13 (12) (1976) 5188.
[25] R. Hundt, et al., Determination of symmetries and idealized cell parameters for simulated structures, J. Appl. Cryst. 32 (3) (1999) 413–416.
[26] A. Hannemann, et al., A new algorithm for space-group determination, J. Appl. Cryst. 31 (6) (1998) 922–928.
[27] A. Hassan, et al., Effect of heteroatoms on structural, electronic and spectroscopic properties of polyfuran, polythiophene and polypyrrole: a hybrid DFT approach, J. Mol. Struct. 1274 (2023) 134484.
[28] H. Yu, et al., Coupling ferroelectric polarization and anisotropic charge migration for enhanced CO2 photoreduction, Appl. Catal. Environ. 284 (2021) 119709.
[29] R. Ullah, et al., Pressure-dependent elasto-mechanical stability and thermoelectric properties of MYbF3 (M= Rb, Cs) materials for renewable energy, Int. J. Energy Res. 45 (6) (2021) 8711–8723.
[30] S. Tabassam, et al., Co2YZ (Y= Cr, Nb, Ta, V and Z= Al, Ga) Heusler alloys under the effect of pressure and strain, J. Mol. Graph. Model. 104 (2021) 107841.
[31] R. Singla, et al., Genesis of magnetism in graphene/MoS2 van der Waals hetero-structures via interface engineering using Cr-adsorption, J. Alloys Compd. 859 (2021) 157776.
[32] D. Hoat, et al., Strain effect on the electronic and optical properties of 2D Tetrahexcarbon: a DFT-based study, Indian J. Phys. (2021) 1–9.
[33] M. Husain, et al., Insight into the physical properties of the inter-metallic titanium-based binary compounds, Eur. Phys. J. Plus 136 (6) (2021) 624.
[34] A. Jain, et al., Commentary: the materials project: a materials genome approach to accelerating materials innovation, APL Mater. 1 (1) (2013).
[35] C. Kurkcu, S. Al, C. Yamcicier, Investigation of mechanical properties of KCaH3 and KSrH3 orthorhombic perovskite hydrides under high pressure for hydrogen storage applications, Eur. Phys. J. B 95 (11) (2022) 180.
[36] A. Gencer, G. Surucu, S. Al, MgTiO3Hx and CaTiO3Hx perovskite compounds for hydrogen storage applications, Int. J. Hydrogen Energy 44 (23) (2019) 11930–11938.
[37] S. Al, N. Cavdar, N. Arikan, Computational evaluation of comprehensive properties of MgX3H8 (X= Sc, Ti and Zr) as effective solid state hydrogen storage materials, J. Energy Storage 80 (2024) 110402.
[38] A. Mera, M.A. Rehman, First-principles investigation for the hydrogen storage properties of AeSiH3 (Ae= Li, K, Na, Mg) perovskite-type hydrides, Int. J. Hydrogen Energy 50 (2024) 1435–1447.
[39] R. Song, et al., First-principles to explore the hydrogen storage properties of XPtH3 (X= Li, Na, K, Rb) perovskite type hydrides, Int. J. Hydrogen Energy 57 (2024) 949–957.
[40] E.N. Koukaras, et al., Phonon properties of graphene derived from molecular dynamics simulations, Sci. Rep. 5 (1) (2015) 12923.
[41] B. Sahoo, K. Joshi, S.C. Gupta, Pressure effect on elastic, lattice dynamic and superconducting behaviour of yttrium sulfide: a first principle study, J. Appl. Phys. 115 (12) (2014).
[42] K. Parlinski, Software phonon, Cracow (2010); K. Parlinski, ZQ Li, Y. Kawazoe, Phys. Rev. Lett. 78 (1997) 4063.
[43] F. Subhan, et al., Elastic and optoelectronic properties of CaTa2O6 compounds: cubic and orthorhombic phases, J. Alloys Compd. 785 (2019) 232–239.
[44] A. Adam, et al., Enhanced thermoelectric figure of merit in Bi-containing Sb2Te3 bulk crystalline alloys, J. Phys. Chem. Solid 138 (2020) 109262.
[45] M. Ali, et al., Ternary boride Hf3PB4: insights into the physical properties of the hardest possible boride MAX phase, J. Alloys Compd. 857 (2021) 158264.
[46] F. Mouhat, F.-X. Coudert, Necessary and sufficient elastic stability conditions in various crystal systems, Phys. Rev. B 90 (22) (2014) 224104.
[47] W. Voigt, Lehrbuch der kristallphysik:(mit ausschluss der kristalloptik) vol. 34, BG Teubner, 1910.
[48] A. Reuß, Berechnung der fließgrenze von mischkristallen auf grund der plastizitätsbedingung für einkristalle, ZAMM-Journal of Applied Mathematics and Mechanics/Zeitschrift für Angewandte Mathematik und Mechanik 9 (1) (1929) 49–58.
[49] R. Hill, First-principles elastic constants for the hcp transition metals Fe, Co, and Re at high pressure, in: *Proc. Phys. Soc.*, 1952.
[50] M. Rajagopalan, S.P. Kumar, R. Anuthama, FP-LAPW study of the elastic properties of Al2X (X= Sc, Y, La, Lu), Phys. B Condens. Matter 405 (7) (2010) 1817–1820.
[51] O.L. Anderson, H.H. Demarest Jr., Elastic constants of the central force model for cubic structures: polycrystalline aggregates and instabilities, J. Geophys. Res. 76 (5) (1971) 1349–1369.
[52] A. Šimůnek, How to estimate hardness of crystals on a pocket calculator, Phys. Rev. B 75 (17) (2007) 172108.
[53] L. Kleinman, Deformation potentials in silicon. *I. Uniaxial strain*, Phys. Rev. 128 (6) (1962) 2614.
[54] Z. Sun, et al., Theoretical investigation of the bonding and elastic properties of nanolayered ternary nitrides, Phys. Rev. B 71 (19) (2005) 193402.
[55] M. Hadi, et al., Physical properties and defect processes of M3SnC2 (M= Ti, Zr, Hf) MAX phases: effect of M-elements, J. Alloys Compd. 748 (2018) 804–813.
[56] M. Roknuzzaman, et al., Physical properties of predicted Ti2CdN versus existing Ti2CdC MAX phase: an ab initio study, Comput. Mater. Sci. 113 (2016) 148–153.
[57] A. Chowdhury, et al., Predicted MAX phase Sc2InC: dynamical stability, vibrational and optical properties, Phys. Status Solidi B 255 (3) (2018) 1700235.
[58] M. Ali, et al., Physical properties of new MAX phase borides M2SB (M= Zr, Hf and Nb) in comparison with conventional MAX phase carbides M2SC (M= Zr, Hf and Nb): comprehensive insights, J. Mater. Res. Technol. 11 (2021) 1000–1018.
[59] M. Ali, et al., DFT insights into new B-containing 212 MAX phases: Hf2AB2 (A= In, Sn), J. Alloys Compd. 860 (2021) 158408.
[60] S. Pugh, XCII., *Relations between the elastic moduli and the plastic properties of polycrystalline pure metals.* The London, Edinburgh, and Dublin philosophical magazine and journal of, Science 45 (367) (1954) 823–843.
[61] M.A. Afzal, S. Naqib, A DFT based first-principles investigation of optoelectronic and structural properties of Bi2Te2Se, Phys. Scr. 96 (4) (2021) 045810.
[62] C.M. Kube, Elastic anisotropy of crystals, AIP Adv. 6 (2016) 9.
[63] P. Ravindran, et al., Density functional theory for calculation of elastic properties of orthorhombic crystals: application to TiSi 2, J. Appl. Phys. 84 (9) (1998) 4891–4904.
[64] S.I. Ranganathan, M. Ostoja-Starzewski, Universal elastic anisotropy index, Phys. Rev. Lett. 101 (5) (2008) 055504.
[65] C.M. Kube, M. De Jong, Elastic constants of polycrystals with generally anisotropic crystals, J. Appl. Phys. 120 (16) (2016).
[66] R. Gaillac, P. Pullumbi, F.-X. Coudert, ELATE: an open-source online application for analysis and visualization of elastic tensors, J. Phys. Condens. Matter 28 (27) (2016) 275201.
[67] O.L. Anderson, A simplified method for calculating the Debye temperature from elastic constants, J. Phys. Chem. Solid 24 (7) (1963) 909–917.
[68] M. Fine, L. Brown, H. Marcus, Elastic constants versus melting temperature in metals, Scr. Metall. 18 (9) (1984) 951–956.
[69] M. Dresselhaus, Solid State Physics. Part II: Optical Properties of Solids. Course 6.732 Solid State Physics, MIT, 1999. http://web.mit.edu/course/6/6.732/www/6.732-pt2. pdf.